PI-RADS Classification: Structured Reporting for MRI of the Prostate

M. Röthke[1]; D. Blondin[2]; H.-P. Schlemmer[1]; T. Franiel[3]

[1]Department of Radiology, German Cancer Research Center (DKFZ), Heidelberg, Germany
[2]Department of Diagnostic and Interventional Radiology, University Hospital Düsseldorf, Germany
[3]Department of Radiology, Charité Campus Mitte, Medical University Berlin, Germany

Introduction

Prostate MRI has become an increasingly common adjunctive procedure in the detection of prostate cancer. In Germany, it is mainly used in patients with prior negative biopsies and/or abnormal or increasing PSA levels. The procedure of choice is multiparametric MRI, a combination of high-resolution T2-weighted (T2w) morphological sequences and the multiparametric techniques of diffusion-weighted MRI (DWI), dynamic contrast-enhanced MRI (DCE-MRI), and proton MR spectroscopy (^{1}H-MRS) [1, 2]. Previously, there were no uniform recommendations in the form of guidelines for the implementation and standardized communication of findings. To improve the quality of the procedure and reporting, a group of experts of the European Society of Urogenital Radiology (ESUR) has recently published a guideline for MRI of the prostate [3]. In addition to providing recommendations relating to indications and minimum standards for MR protocols, the guideline describes a structured reporting scheme (PI-RADS) based on the BI-RADS classification for breast imaging. This is based on a Likert scale with scores ranging from 1 to 5. However, it lacks illustration of the individual manifestations and their criteria as well as uniform instructions for aggregated scoring of the individual submodalities. This makes use of the PI-RADS classification in daily routine difficult, especially for radiologists who are less experienced in prostate MRI. It is therefore the aim of this paper to concretize the PI-RADS model for the detection of prostate cancer using representative images for the relevant scores, and to add a scoring table that combines the aggregated multiparametric scores to a total PI-RADS score according to the Likert scale. In addition, a standardized graphic prostate reporting scheme is presented, which enables accurate communication of the findings to the urologist. Furthermore, the individual multiparametric techniques are described and critically assessed in terms of their advantages and disadvantages.

Materials and methods

The fundamentals of technical implementation were determined by consensus. The sample images were selected by the authors by consensus on the basis of representative image findings from the 3 institutions. The scoring intervals for the aggregated PI-RADS score were also determined by consensus. The individual imaging aspects were described and evaluated with reference to current literature by one author in each case (T2w: M.R., DCE-MRI: T.F., DWI: D.B., MRS: H.S.). Furthermore, a graphic reporting scheme that allows the findings to be documented in terms of localization and classification was developed, taking into account the consensus paper on MRI of the prostate published in 2011 [4].

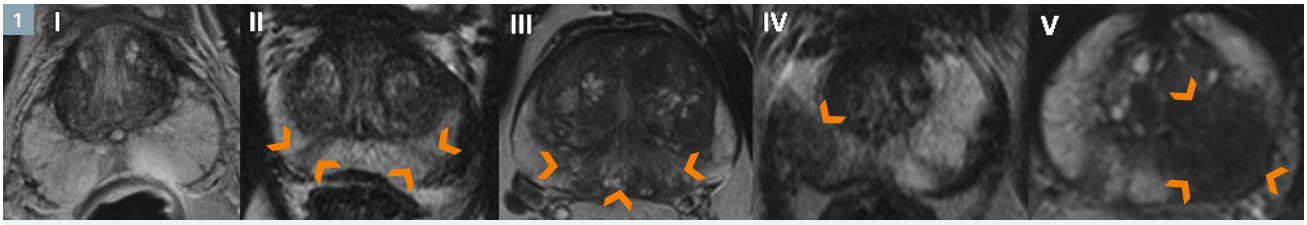

I	II	III	IV	V
I: Normal PZ in T2w hyperintense	II: Hypointense discrete focal lesion (wedge or band-shaped, ill-defined)	III: Changes not falling into categories 1+2 & 4+5	IV: Severely hypointense focal lesion, round-shaped, well-defined without extracapsular extension	V: Hypointense mass, round and bulging, with capsular involvement or seminal vesicle invasion

1 PI-RADS classification of T2w: peripheral glandular sections.

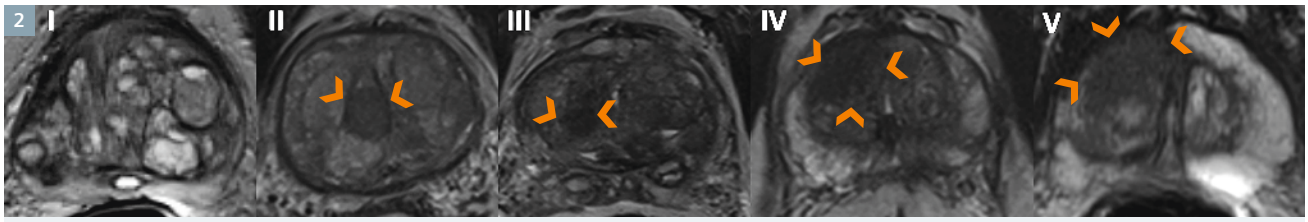

I	II	III	IV	V
I: TZ with stromal & glandular hyperplasia without focal hypointense nodular or oval-shaped	II: Round hypointense lesion with signs of well-defined capsule. Band-shaped hypointense regions	III: Changes not falling into categories 1+2 & 4+5	IV: Oval-shaped anterior hypointense lesion without evidence of capsular involvement, "charcoal sign": homogeneous hypointense lesions with loss of matrix + ill-defined margins	V: Oval-shaped or round mass with compression/retraction/ extension of the anterior capsule. Irregular, infiltrating mass with architectural disintegration, invasion into adjacent structures

2 PI-RADS classification of T2w: central glandular sections.

Implementation and technical requirements

According to the German interdisciplinary S3 guideline for prostate cancer, MRI of the prostate should be performed on a high-field scanner with a minimum field strength of 1.5 Tesla (T) using a combined endorectal-body phased-array coil in order to ensure a high signal-to-noise ratio in the prostate region [5]. If using 3T scanners and conventional MRI in combination with at least 2 multiparametric techniques, an endorectal coil is not mandatory for the detection and localization of prostate cancer in our opinion. While administration of spasmolytics such as butylscopolamine is helpful in order to reduce intestinal peristalsis, we do not consider it essential [6].

Morphological T2w imaging

The high-resolution T2w turbo-spin-echo (TSE) sequences are the basis of MRI imaging of the prostate. T2w imaging visualizes morphological information of the prostate. A diagnostic challenge lies in the non-specific visualization of different but morphologically similar entities such as post-inflammatory or post-biopsy scars, atrophic changes, prostatitis, intraepithelial neoplasias (PIN), or post-treatment lesions [3]. The probability of detection decreases with decreasing size of the lesions [7].

In patients aged 50 years and older, the transition zone is increasingly affected by nodular changes from benign prostatic hyperplasia (BPH), which complicate the detection of prostate cancer [8]. On the T2w images, the BPH nodules show different signal behaviors depending on the size of the epithelial and stromal components. While the epithelial component shows a hyperintense and the stromal component a hypointense signal behavior, combinations of both changes can also be seen. The BPH nodules are characterized by septation of the individual nodules, which can be seen as a hypointense rim on the T2w images [9]. Severely hypointense areas are non-specifically suggestive of prostate cancer [10]. Due to their infiltrating growth, aggressive prostate cancers in the central glandular zone spread across the septal structures, which is referred to as 'charcoal sign' [8]. Larger cancers of the central glandular zone also have a space-occupying component as a sign of malignancy. Aggressive cancers tend to have a more hypointense signal intensity with increasing Gleason score (≥ 7) [11].

At least 75% of all prostate cancers occur in the peripheral zone, where they appear localized and, when visualized by T2w imaging, predominantly distinctly hypointense compared to the hyperintense glandular tissue of the peripheral zone [12]. A visible space-occupying component or extracapsular extension must be interpreted as a reliable sign of malignancy. Smaller cancers can be localized, but have irregular borders and finger-like processes. The cancer-specific changes shown on T2w images must be differentiated from the diffuse inflammatory contrasts caused by chronic prostatitis [13]. These can consist of mildly to severely hypointense diffuse changes which may be unilaterally localized, but may also affect the periphery on both sides. At the cicatricial stage, they consist of streaky changes which typically appear as triangular areas extending from the capsule to the apical/urethral margin. Less frequently than with diffuse changes, granulomatous prostatitis presents focal hypointense areas which can mimic prostate carcinoma. Post-biopsy hemorrhages (generally 3 – 6 months following biopsy) also appear hypointense on T2w, but hyperintense on T1w images. Previously biopsied areas may appear as scarred, strand-like hypo-intense changes on T2w images. Special attention must be paid to the rectoprostatic angle, since obliteration of the angle or asymmetry are indicative of extracapsular carcinoma [14].

The T2-weighted TSE sequence is acquired in the axial plane and complemented by a sagittal and/or coronal sequence. In addition to the T2w sequences, an axial T1w sequence should be acquired in order to visualize intraprostatic bleeding from inflammation or prior biopsies and, using an extended field-of-view (FOV), to detect enlarged parailiac and

locoregional lymph nodes suggestive of metastases. The high-resolution T2w sequences should have an echo time (TE) of 100 – 120 ms and a long repetition time (TR) of 4000 – 8000 ms (depending on the equipment and B_0 field strength). Parallel imaging may be used. A minimum slice thickness of 4 mm at 1.5 Tesla or 3 mm at 3 Tesla should be used, and a minimum in-plane resolution of 0.7 × 0.7 mm for both field strengths.

PI-RADS classification of T2w imaging

Since the diagnostic significance of the T2w-TSE sequences differs for the peripheral and central glandular zone, 2 separate schemes are recommended. Each lesion is given a score on a scale of 1 to 5. In the peripheral zone, in particular inflammatory lesions must be differentiated from lesions suspicious of cancer (Fig. 1). Lesions in the central glandular sections must be differentiated from clearly benign BPH nodules (Fig. 2). In addition, the presence of extracapsular extension, seminal vesicle invasion or involvement of the bladder neck must be documented [15].

Diffusion-weighted imaging

DWI allows the visualization and analysis of the movement (diffusion) of water molecules in the intracellular space. Molecular diffusion in tissue is generally restricted by cell structures and membranes. DWI allows the visualization and analysis of the movement (diffusion) of water molecules and expresses it by a parameter known as the apparent diffusion coefficient (ADC). Molecular diffusion in tissue is generally restricted by cell structures and membranes. Intracellular edemas or higher cell densities lead to a further reduction of free molecular movement. Such restrictions are reflected by a reduced ADC value. High cell densities occur, e.g., in tumor tissue, and thus also prostate carcinoma is characterized by reduced ADC values [16, 17]. Intracellular edemas or higher cell densities lead to a further reduction of free molecular movement, which is reflected by a reduced ADC value.

Consequently, prostate carcinoma is also characterized by reduced ADC values [16, 17]. In nearly all previously published studies, the ADC was analyzed using a mono-exponential model. As yet there have been only few publications on bi-exponential ADC analysis for the prostate [18, 19]. Therefore, the significance of the bi-exponential analysis, the static model, DTI or kurtosis [20 – 22] in the diagnosis of prostate cancer cannot be evaluated conclusively at this time. To allow the widespread use of DWI in multiparametric prostate MRI, the method used for calculation and analysis of the ADC should be practical, time-efficient and, above all, standardized. Several studies have shown that DWI analyzed with a mono-exponential model increases the sensitivity and specificity of detection of prostate cancer and allows better differentiation from benign hyperplasia [23 – 26]. The published ADC data are, however, inconsistent. The variations in the ADC results are due to different field strengths and different numbers and magnitudes of the selected b-values [27]. The most frequently used upper b-values are b = 500, b = 800 or b = 1000 s/mm². The guidelines recommend an upper value of b = 800 – 1000 s/mm². The authors prefer a value of 1000, which does, however, not deliver sufficient results with all gradient systems. In a study performed at 1.5T, the highest diagnostic accuracy in the detection of prostate cancer was achieved with a combination of T2 and DWI with an upper b-value of b = 2000 s/mm² and using a surface coil [28]. For 3 Tesla exams, the use of an upper b-value of 2000 s/mm² cannot currently be recommended unequivocally [26], even though a current published study was able to demonstrate a benefit with b = 2000 at 3 Tesla [29].

Prostate carcinomas usually show reduced ADC values and high signal intensity in the high-b-value image from DWI. In addition, the ADC values had negative correlation with the Gleason score of peripheral zone carcinomas. A significant difference was observed with tumors with a Gleason score of 6 compared to those with a score of 7 or 8. There was no significant difference between tumors with a Gleason score ≥ 7 [30]. Other authors also demonstrated a linear reduction of the ADC of peripheral zone prostate carcinoma with increasing Gleason score and significant differences between low-grade, intermediate and high-grade PCa [31]. Even though there is not an exact correspondence of ADC thresholds and Gleason scores, DWI is still the most important tool in the detection of the most aggressive lesion (index lesion).

DWI should be performed with an echoplanar (EPI) sequence in the same axial orientation as the T2w imaging. The diffusion gradients should be applied in 3 orthogonal spatial directions. As a minimum 3, ideally 5, b-values between 0 and 800 – 1000 s/mm² should be used. Echo time should be as short as possible (typically < 90 ms). The sequence is prone to susceptibility artifacts, which can lead to distortions of the DWI images due to adjacent bowel gas. The measurement of the restricted diffusion in tumor tissue using high b-values improves the MRI diagnosis of prostate cancer.

PI-RADS classification of DWI

DWI is interpreted based on the high-b-value images (b ≥ 800 s/mm²) and the corresponding ADC parametric images (Fig. 3). A score of 1 is assigned if no focal decrease in signal intensity can be delineated on the ADC images, and no localized increase in signal intensity on the DWI images. Two points should be assigned for diffuse hyperintensities on the high-b-value image of the DWI with corresponding reduction of the ADC. This includes diffuse (e.g. triangular or linear) changes; focal, round areas are disregarded. Three points are assigned for unilateral (asymmetric) diffuse signal increase on the high-b-value image, which is diffusely decreased on the ADC map (no focality).

Four points are given for focal lesions that are clearly reduced on the ADC map, but are isointense on the high-b-value DWI image. Focal ADC reductions with corresponding focal signal increase on the DWI image (b ≥ 800 s/mm²) should be assigned 5 points.

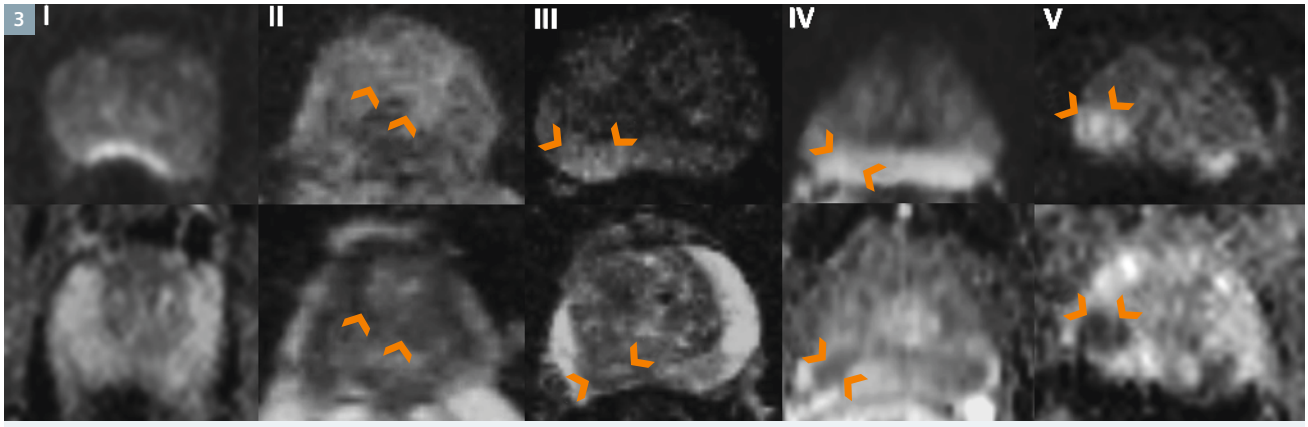

I	II	III	IV	V
I: No reduction in ADC compared with normal tissue / no increase in SI on ≥ b800 images	II: Diffuse hyperintensity on ≥ b800 image with low ADC, no focal lesions: linear, triangular or diffuse areas permitted	III: Unilateral hyperintensity on ≥ b800 image with diffuse reduced ADC (no focal lesions)	IV: Focal area with reduced ADC but isointense SI on ≥ b800 image	V: Focal hyperintense area/mass on ≥ b800 image with reduced ADC

3 PI-RADS classification of DWI (high b-values and ADC).

For each evaluated lesion, an ADC value should be determined by ROI measurement and documented in the report. This quantitative ADC analysis depends on the magnetic field strength and the selected b-values. ADC limits should therefore be transferred or applied with caution [17]. Nevertheless, a high ADC value of >1000 10^{-3} mm²/s is most likely to represent an inflammatory area or hyperplasia, and a significantly reduced ADC value of < 600 10^{-3} mm²/s a tumor.

DCE-MRI

DCE-MRI is a non-invasive technique that collects information on the vascularization of the prostate and the neoangiogenesis of prostate cancer [32]. DCE-MRI usually measures T1w signal intensity(SI)-time(t) curves in the prostate tissue following the weight-adjusted administration of a gadolinium-based contrast medium (CM) in a bolus at an injection rate of 2.5 ml/s and subsequent injection of 20 ml of isotonic NaCl [2, 32]. For this, axial gradient echo sequences should be used. The temporal resolution should be at least 10 s (better ≤ 4 s to adequately follow the contrast medium through the tissue). To allow sufficient assessment of the SI-t curve, the sequence should be at least 5 min. long. Spatial resolution should be 0.7 x 0.7 mm² to 1.0 x 1.0 mm² at a slice thickness of 3 mm (distance factor 0.2). Alternatively, with 3 Tesla, isotropic voxels with a size of $(1.5\ mm)^3$ can be generated, and optionally additional multiplanar reconstructions. The SI measurements enable a qualitative and semi-quantitative analysis of the DCE-MRI data. The qualitative analysis is based on the course of the SI-t curve. For the semi-quantitative analysis, a continuous SI-t curve is generated from the SI plotted over time. Based on this, the time to initial enhancement in the prostate tissue, the rise of the SI-t curve (wash-in), the maximum SI, and the fall of the SI-t curve (wash-out) is calculated [33]. Quantitative analysis of the DCE-MRI data by means of pharmacokinetic parameters requires conversion of the SI to CM concentrations [34]. The techniques and sequences used for this have recently been described in detail [2, 32]. The increasingly preferred pharmacokinetic model is the two-compartment model with the exchange constants K^{trans} (transfer constant) and k_{ep} (rate constant) [34].

Combined with conventional T1w and T2w imaging, DCE-MRI can detect and localize prostate cancer with better accuracy than conventional MRI [35 – 38], with the degree of improvement evidently depending on the experience of the reader.

In the qualitative analysis, prostate cancers typically show a steeper wash-in slope, higher peak enhancement and steeper wash-out compared to normal prostate tissue. This correlates with the semiquantitative analysis, where prostate carcinoma tends to exhibit higher values of the individual parameter values as well [39, 40]. In the quantitative analysis, the pharmacokinetic parameters K^{trans} and k_{ep} also have higher values than normal prostate tissue [41].

In terms of differential diagnosis, prostatitis cannot be clearly differentiated from prostate cancer [42]. Similarly, it is not possible to reliably differentiate BPH nodules from central gland prostate cancers. The cause of false negative findings are prostate cancers which do not, or not significantly, differ from the surrounding normal tissue in terms of the degree of vascularization.

Based on current knowledge, no reliable recommendation can be made for assessing the aggressiveness of prostate cancer with DCE-MRI [4]. To date, only one study has demonstrated that low-grade prostate cancers were characterized by a statistically significantly larger blood volume and lower permeability than high-grade prostate cancers [43].

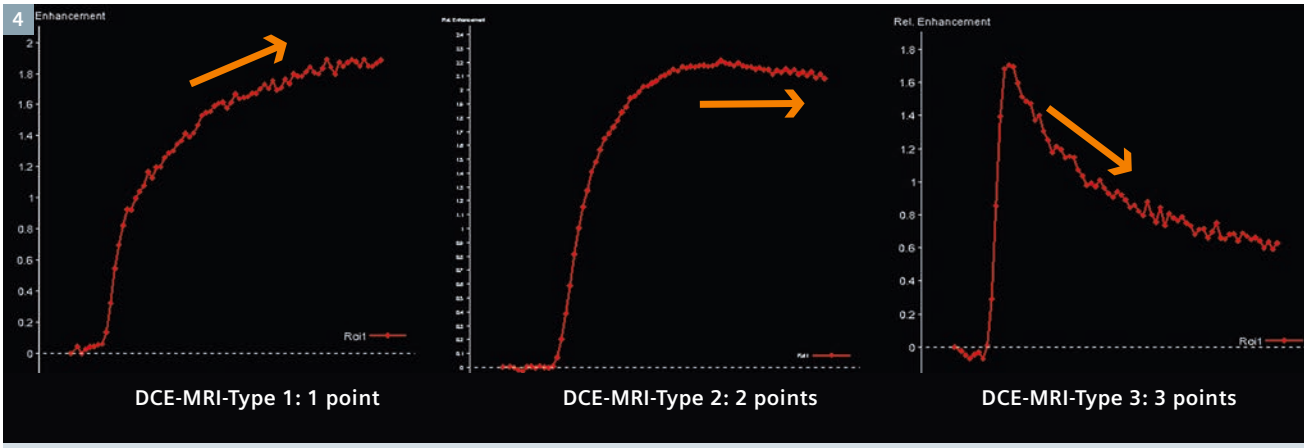

4 PI-RADS classification of DCE-MRI, part 1: Curve types.

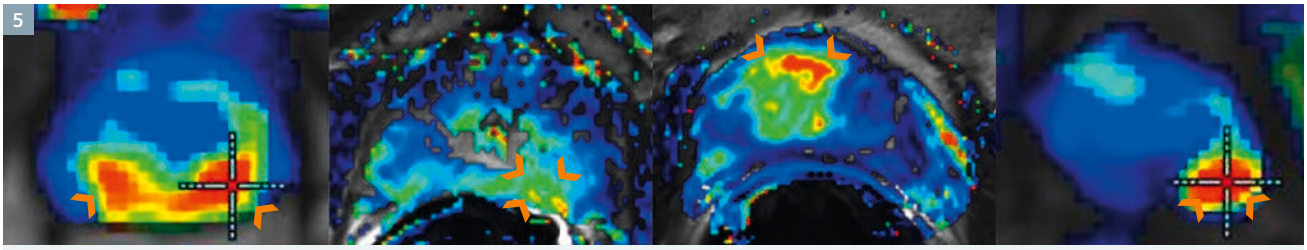

5 PI-RADS classification of DCE-MRI, part 2: Additional points for distribution patterns with curve types II + III.

PI-RADS classification of DCE-MRI

The SI-t curves measured by DCE-MRI are the basis for the PI-RADS classification, the key element being the qualitative analysis of the curve shape following the initial rise of the SI-t curve (Fig. 4). In a type I curve, the SI gradually continues to increase (score 1). Type II curves are characterized by progressive SI stabilization (curve levels off) and a slight and late decrease in SI (score 2).

Type III curves show immediate washout after reaching peak enhancement (score 3). A point is added in the scoring system if there is a focal lesion with a type II or type III curve (Fig. 5). Another point is added for asymmetric lesions or unusually located lesions with type II or type III curves [3]. Unusual locations are the anterior parts of the transition zone and the anterior horns of the peripheral zone. Symmetry and focality are assessed based on the surrounding tissue. In practice, it is helpful (although not mandatory) to assess focality by means of pharmacokinetic parameter maps. If new lesions are identified in the analysis of the pharmacokinetic parameter maps, these areas can also be assessed using the PI-RADS classification scheme. Here it must be noted that BPH nodules appear as focal lesions on the parameter maps and are characterized by type II or type III curves. No classification is necessary for lesions that can be clearly diagnosed as BPH nodules on the T2w image due to their hypointense rim.

MR spectroscopy of the prostate

Proton magnetic resonance spectroscopy allows the spatially resolved measurement of the relative concentration distributions of the metabolites citrate, creatine and choline in the prostate. This metabolic information can increase the specificity of morphological prostate MRI and help assess individual tumor aggressiveness [44] and its progression over time, e.g. following antihormonal therapy [45] or during active surveillance [46].

Three-dimensional spatially resolved proton MR spectroscopy imaging (^{1}H-MRSI) is generally performed using a combination of two techniques, namely point resolved spectroscopy (PRESS) for volume-selective excitation, and chemical shift imaging (^{1}H-CSI) for spatial resolution with voxel sizes of up to 0.25 cm^3. ^{1}H-MRSI is technically more complex than MR tomographic imaging and has several limitations in routine practice [47, 48]. Due to the high water content of human tissue, the proton, i.e. the nucleus of the most common hydro-

gen isotope (^{1}H), is the *in-vivo* nucleus that provides the strongest signal. Within the prostate parenchyma, the concentration of citrate, creatine and choline is approx. 10,000- to 100,000-fold lower than that of water. The signal intensity of these metabolite resonances in the ^{1}H-MR spectrum is thus reduced by the same factor, which complicates their visualization using this method. It is nevertheless possible to measure the resonances of the metabolites citrate, creatine and choline with only low signal-to-noise ratio. This requires a water and fat signal suppression pulse to enable the detection of the weak resonance lines of the metabolites against the background of the strong water signal on the one hand, and to suppress contamination of the spectra by signal from periprostatic lipids on the other hand. In addition, wide saturation bands must be placed closely around the prostate in order to suppress the strong water and fat signals from the surrounding tissue. Spectral quality critically depends on the local magnetic field homogeneity, which must be optimized prior to the data acquisition by automatic and possibly additional manual shimming. The total duration of the exam is approx. 10 – 15 min.

MRSI is evaluated by determining the relative signal intensity ratios of the resonance lines [choline + creatine]/citrate (CC/C). Since the choline and creatine resonances often cannot be resolved due to field inhomogeneities and consecutive line broadening, they are combined into one line (CC). The quality of the spectra should initially be assessed visually on a spectral map. For semiquantitative analysis of the spectra, manufacturers are offering partly interactive software. To avoid partial volume effects, it may be necessary to retrospectively shift the voxel grid to adapt it to the precise anatomic localization of focal lesions.

The MRSI procedure, including data acquisition, evaluation and interpretation of the spectra as well as documentation of the results, requires special expertise and a considerable amount of time (e.g. placement of saturation pulses, possibly manual shimming, interactive data evaluation and interpretation including quality assessment, visualization of results). The quality of the MRSI result depends not only on the physical-technical support, but also on the particular equipment (field strength, equipment generation, specific equipment properties, use of an endorectal coil) and the individual patient-specific examination setting (post-biopsy hemorrhage, possibly regional metal implants such as hip joint endoprosthesis or postoperative metal clips).

Citrate (C) is synthesized, secreted and stored in large quantities in normal glandular tissue of the prostate and is therefore used as an organ marker for healthy prostate tissue. Creatine plays an important role in the cells' energy metabolism and serves as an internal reference of intensity. Choline refers to the sum of choline-containing compounds, which includes various free choline compounds such as phosphocholine, glycerophosphocholine, free choline, CDP-choline, acetylcholine and choline plasmalogen. The intensity of the choline resonance reflects the extent of membrane turnover and is significantly elevated in cancerous tissue [49]. The spatial distribution of relative signal intensity can be visualized through parameter maps and overlaid on the morphological T2w image as a color-coded map. MRSI does not provide any additional information on the localization of the cancer prior to radical prostatectomy as compared to conventional MRI [50]. Due to possible false negative results, in particular with small cancers, ^{1}H-MRSI also cannot be used to exclude cancer. Neither does MRS provide any additional information for local T-staging compared to MRI. Rather, it should be seen as an adjunctive tool to MRI that can increase the specificity in the classification of suspicious focal lesions, assess individual tumor aggressiveness, and provide progression parameters during active surveillance or conservative management. Compared to MRI, however, this method is more complex, more susceptible to artifacts and more difficult to standardize, resulting in it being of low practicality and acceptance outside specialized centers, and thus less commonly used.

PI-RADS classification ^{1}H-MRSI

In regard to the PI-RADS classification of the MR spectroscopy results, qualitative assessment of the CC/C ratio has proven useful in clinical routine. This involves the visual classification of relative signal intensities of the choline and citrate resonances based on a 5-point scale [51, 52]: Type 1: Cho is significantly lower than citrate (<<); type 2: Cho is elevated but still lower than citrate (<); type 3: Cho is approx-

6

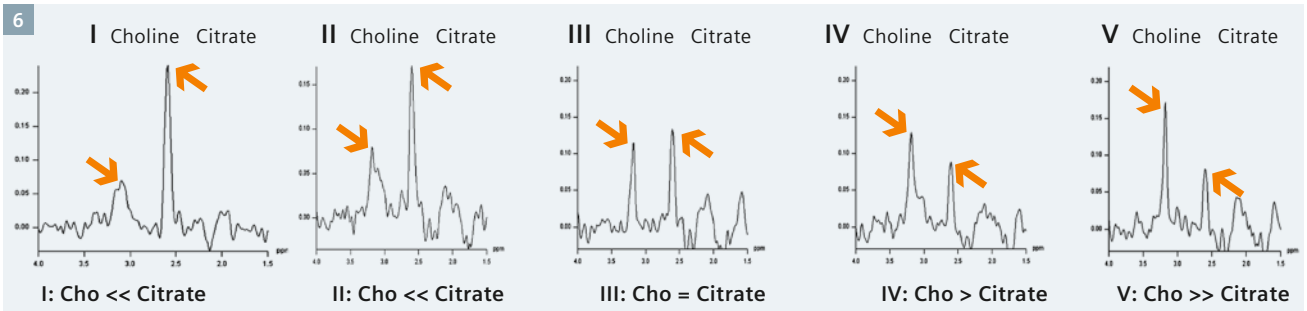

6 PI-RADS classification of MR spectroscopy.

imately on the same level as citrate (=); type 4: Cho is elevated compared to citrate (>); type 5: Cho is significantly elevated compared to citrate (>>) (Fig. 6). Quantitative signal intensity ratios depend on the examination technique (1.5T versus 3T, sequence parameters), the evaluation program used and, in the case of interactive evaluation, examiner-related factors. Quantitative values for classifying the probability of cancer can only be determined in specialized centers and compared within a patient population examined and evaluated by consensus.

Sources of false positive findings are regions with either reduced citrate levels (in the anterior fibromuscular stroma and in stromal BPH nodules) or elevated choline levels (basal near the seminal vesicles and periurethral, since the seminal fluid contains elevated levels of glycerophosphocholine, as well as in prostatitis). False negative findings can occur with small or infiltrating carcinomas, in particular mucous carcinomas.

Communication of findings

In analogy to the BI-RADS, the PI-RADS system offers the advantage of a standardized and easy communication of findings to other professional colleagues. Every lesion should be evaluated using a standardized graphic prostate scheme (Fig. 7) with at least 16, better 27, sectors. For each lesion, a point score between 1 and 5 is to be assigned per method. This is used to calculate the total score, which reflects the probability of the presence of clinically relevant cancer. The total score is then converted to the relevant PI-RADS score, providing the advantage that the final PI-RADS score is independent of the number of techniques used and can thus be easily communicated. Since the conversion of point scores is not explicitly explained in the ESUR guidelines, the authors recommend using the algorithm given in (Table 1). For routine clinical work, the authors further recommend that a diagnosis of suspected prostate cancer should be made if the PI-RADS score is 4 (≥ 10 points if 3 techniques are used and ≥ 13 points if 4 techniques are used) or higher. It must be stressed in this context that the thresholds of 10 and 13 are not yet evidence-based. A lower total score does not mean that the probability of prostate cancer is nil. These patients should therefore at least remain under clinical surveillance.

Conclusion

In summary, structured reporting of a lesion using the parametric approach increases the quality and diagnostic value of prostate MRI. Therefore, application of the PI-RADS scheme based on the representative images provided here is recommended for clinical rou-

7

Standardized MRI Reporting Scheme

Name: _____
Date:
PSA:
Previous Biopsies:
Previous MRI scans:

Individual Scoring

Region	T2	DWI	DCE	MRS	Sum	PI-RADS

Total score PI-RADS:
PI-RADS: 1 – benign; 2 – most probably benign;
3 – intermediate; 4 – probably malignant;
5 – highly suspicious of malignancy

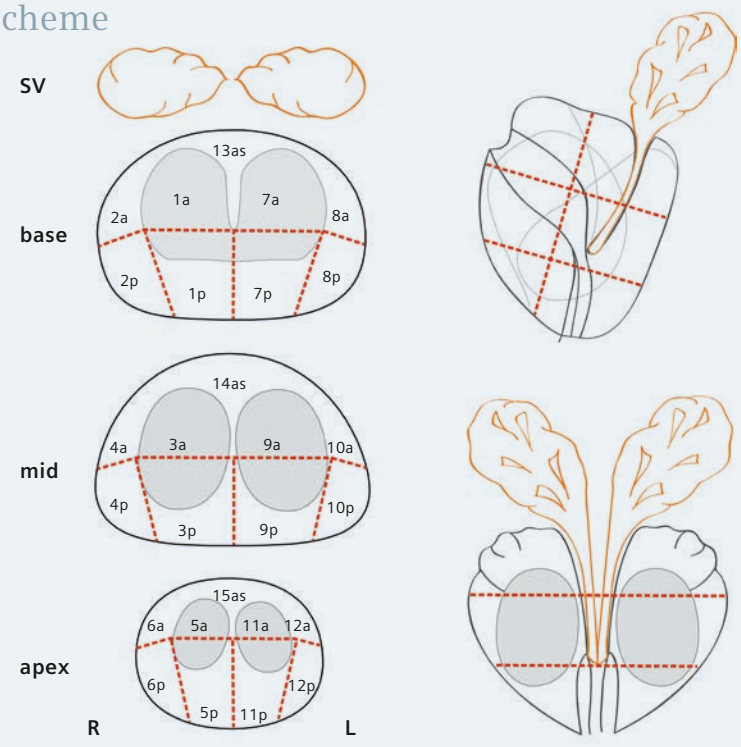

7 Standardized MRI prostate reporting scheme, PI-RADS.
Parts of Fig. 7 are based on Dickinson et al. 2011 [4].

Table 1: PI-RADS score: Definition of total score and assignment of aggregate scores according to individual modalities used.

PI-RADS classification	Definition	Total score with T2, DWI, DCE	Total score with T2, DWI, DCE and MRS
1	most probably benign	3, 4	4, 5
2	probably benign	5, 6	6 – 8
3	indeterminate	7 – 9	9 – 12
4	probably malignant	10 – 12	13 – 16
5	highly suspicious of malignancy	13 – 15	17 – 20

tine. The standardized graphic reporting scheme facilitates the communication with referring colleagues. Moreover, a standardized reporting system not only contributes to quality assurance, but also promotes widespread use of the method and implementation of large-scale multicenter studies, which are needed for further evaluation of the PI-RADS system, in analogy to the BI-RADS system used in breast imaging.

This article has been reprinted with permission from: M. Röthke, D. Blondin, H.-P. Schlemmer, T. Franiel, PI-RADS-Klassifikation: Strukturiertes Befundungsschema für die MRT der Prostata Fortschr Röntgenstr 2013; 185(3): 253-261, DOI: 10.1055/s-0032-1330270 © Georg Thieme Verlag KG Stuttgart New York.

References

1 Schlemmer HP. Multiparametric MRI of the prostate: method for early detection of prostate cancer? Fortschr Röntgenstr 2010; 182: 1067–1075. DOI: 10.1055/s-0029-1245786.
2 Franiel T.Multiparametric magnetic resonance imaging of the prostate – technique and clinical applications. Fortschr Röntgenstr 2011; 183:607–617. DOI: 10.1055/s-0029-1246055.
3 Barentsz JO, Richenberg J, Clements R et al. ESUR prostateMR guidelines 2012. Eur Radiol 2012; 22: 746–757. DOI: 10.1007/s00330-011-2377-y.
4 Dickinson L, Ahmed HU, Allen C et al. Magnetic resonance imaging for the detection, localisation, and characterisation of prostate cancer: recommendations from a European consensus meeting. European urology 2011; 59: 477–494. DOI: 10.1016/j.eururo.2010.12.009.
5 Krebsgesellschaft D. Interdisziplinäre Leitlinie der Qualität S3 zur Früherkennung, Diagnose und Therapie der verschiedenen Stadien des Prostatakarzinoms. 2011.
6 Wagner M, Rief M, Busch J et al. Effect of butylscopolamine on image quality in MRI of the prostate. Clin Radiol 2010; 65: 460–464. DOI: S0009-9260(10)00106-6.
7 Roethke MC, Lichy MP, Jurgschat L et al. Tumorsize dependent detection rate of endorectal MRI of prostate cancer – a histopathologic correlation with whole-mount sections in 70 patients with prostate cancer. Eur J Radiol 2011; 79: 189–195. DOI: S0720-048X(10)00045-8.
8 Akin O, Sala E, Moskowitz CS et al. Transition zone prostate cancers: features, detection, localization, and staging at endorectal MR imaging. Radiology 2006; 239: 784–792. DOI: 2392050949.
9 Janus C, Lippert M. Benign prostatic hyperplasia: appearance on magnetic resonance imaging. Urology 1992; 40: 539–541.
10 Oto A, Kayhan A, Jiang Y et al. Prostate cancer: differentiation of central gland cancer from benign prostatic hyperplasia by using diffusion-weighted and dynamic contrast-enhanced MR imaging. Radiology 2010; 257: 715–723. DOI: radiol.1010002.
11 Wang L, Mazaheri Y, Zhang J et al. Assessment of biologic aggressiveness of prostate cancer: correlation of MR signal intensity with Gleason grade after radical prostatectomy. Radiology 2008; 246: 168–176. DOI: 2461070057.
12 Hricak H. Imaging prostate cancer. J Urol 1999; 162: 1329–1330.
13 Kim CK, Park BK, Kim B. Localization of prostate cancer using 3T MRI: comparison of T2-weighted and dynamic contrast-enhanced imaging. J Comput Assist Tomogr 2006; 30: 7–11. DOI: 00004728-200601000-00002 [pii].
14 Beyersdorff D, Taymoorian K, Knosel T et al. MRI of prostate cancer at 1.5 and 3.0 T: comparison of image quality in tumor detection and staging. Am J Roentgenol 2005; 185: 1214–1220. DOI: 10.2214/AJR.04.1584.
15 Roethke MC, Lichy MP, Kniess M et al. Accuracy of preoperative endorectal MRI in predicting extracapsular extension and influence on neurovascular bundle sparing in radical prostatectomy. World J Urol 2012. DOI: 10.1007/s00345-012-0826-0.
16 Zelhof B, Pickles M, Liney G et al. Correlation of diffusion-weighted magnetic resonance data with cellularity in prostate cancer. BJU Int 2009; 103: 883–888.
17. Sato C, Naganawa S, Nakamura T et al. Differentiation of noncancerous tissue and cancer lesions by apparent diffusion coefficient values in transition and peripheral zones of the prostate. J Magn Reson Imaging 2005; 21: 258–262. DOI: 10.1002/jmri.20251.
18 Mulkern RV, Barnes AS, Haker SJ et al. Biexponential characterization of prostate tissue water diffusion decay curves over an extended b-factor range. Magn Reson Imaging 2006; 24: 563–568.
19 Quentin M, Blondin D, Klasen J et al. Comparison of different mathematical models of diffusion-weighted prostate MR imaging. Magnetic resonance imaging 2012. DOI: 10.1016/j.mri.2012.04.025.
20 Le Bihan D, Breton E, Lallemand D et al. Separation of diffusion and perfusion in intravoxel incoherent motion MR imaging. Radiology 1988; 168: 497–505.
21 Yablonskiy DA, Bretthorst GL, Ackerman JJH. Statistical model for diffusion attenuated MR signal. Magn Reson Med 2003; 50: 664–669.
22 Jensen JH, Helpern JA, Ramani A et al. Diffusional kurtosis imaging: the quantification of non-gaussian water diffusion by means of magnetic resonance imaging. Magn Reson Med 2005; 53: 1432–1440.
23 Haider MA, van der Kwast TH, Tanguay J et al. Combined T2-weighted and diffusion-weighted MRI for localization of prostate cancer. Am J Roentgenol 2007; 189: 323–328.
24 Pickles MD, Gibbs P, Sreenivas M et al. Diffusion-weighted imaging of normal and malignant prostate tissue at 3.0T. J Magn Reson Imaging 2006; 23: 130–134.

25 Ren J, Huan Y,Wang H et al. Diffusion-weighted imaging in normal prostate and differential diagnosis of prostate diseases. Abdom Imaging 2008; 33: 724–728.
26 Kim CK, Park BK, Kim B. High-b-value diffusion-weighted imaging at 3T to detect prostate cancer: comparisons between b values of 1,000 and 2,000 s/mm². Am J Roentgenol 2010; 194: 33–37. DOI: 194/1/W33.
27 Mueller-Lisse UG, Mueller-Lisse UL, Zamecnik P et al. Diffusion-weighted MRI of the prostate. Radiologe 2011; 51: 205–214.
28 Katahira K, Takahara T, Kwee TC et al. Ultra-high-b-value diffusion-weighted MR imaging for the detection of prostate cancer: evaluation in 201 cases with histopathological correlation. Eur Radiol 2011; 21:188–196.
29 Kitajima K, Takahashi S, Ueno Y et al. Clinical utility of apparent diffusion coefficient values obtained using high b-value when diagnosing prostate cancer using 3 tesla MRI: Comparison between ultra-high b-value (2000 s/mm²) and standard high b-value (1000 s/mm²). J Magn Reson Imaging 2012. DOI: 10.1002/jmri.23627.
30 Woodfield CA, Tung GA, Grand DJ et al. Diffusion-weighted MRI of peripheral zone prostate cancer: comparison of tumor apparent diffusion coefficient with Gleason score and percentage of tumor on core biopsy. Am J Roentgenol 2010; 194: 316–322.
31 Vargas HA, Akin O, Franiel T et al. Diffusion-weighted endorectal MR imaging at 3T for prostate cancer: tumor detection and assessment of aggressiveness. Radiology 2011; 259: 775–784. DOI: 10.1148/radiol.11102066.
32 Franiel T, Hamm B, Hricak H. Dynamic contrast-enhanced magnetic resonance imaging and pharmacokinetic models in prostate cancer. Eur Radiol 2011; 21: 616–626. DOI: 10.1007/s00330-010-2037-7.
33 Huisman HJ, Engelbrecht MR, Barentsz JO. Accurate estimation of pharmacokinetic contrast-enhanced dynamic MRI parameters of the prostate. J Magn Reson Imaging 2001; 13: 607–614.
34 Tofts PS, Brix G, Buckley DL et al. Estimating kinetic parameters from dynamic contrast-enhanced T(1)-weighted MRI of a diffusable tracer: standardized quantities and symbols. J Magn Reson Imaging 1999; 10:223–232.
35 Beyersdorff D, Ludemann L, Dietz E et al. Dynamic contrast-enhanced MRI of the prostate: comparison of two different post-processing algorithms. Fortschr Röntgenstr 2011; 183: 456–461. DOI: 10.1055/s-0029-1246051.
36 Franiel T, Stephan C, Erbersdobler A et al. Areas Suspicious for Prostate Cancer: MR-guided Biopsy in Patients with at Least One Transrectal US-guided Biopsy with a Negative Finding – Multiparametric MR Imaging for Detection and Biopsy Planning. Radiology 2011. DOI: radiol.10101251.
37 Ocak I, BernardoM, Metzger G et al. Dynamic contrast-enhanced MRI of prostate cancer at 3 T: a study of pharmacokinetic parameters. Am J Roentgenol 2007; 189: 849.
38 Sciarra A, Panebianco V, Ciccariello M et al. Value of magnetic resonance spectroscopy imaging and dynamic contrast-enhanced imaging for detecting prostate cancer foci in men with prior negative biopsy. Clin Cancer Res 2010; 16: 1875–1883.
39 Engelbrecht MR, Huisman HJ, Laheij RJ et al. Discrimination of prostate cancer from normal peripheral zone and central gland tissue by using dynamic contrast-enhanced MR imaging. Radiology 2003; 229: 248–254.
40 Padhani AR, Gapinski CJ, Macvicar DA et al. Dynamic contrast enhanced MRI of prostate cancer: correlationwith morphology and tumour stage, histological grade and PSA. Clin Radiol 2000; 55: 99–109.
41 Schlemmer HP, Merkle J, Grobholz R et al. Can pre-operative contrast-enhanced dynamic MR imaging for prostate cancer predict microvessel density in prostatectomy specimens? Eur Radiol 2004; 14: 309–317.
42 Franiel T, Lüdemann L, Rudolph B et al. Evaluation of normal prostate tissue, chronic prostatitis, and prostate cancer by quantitative perfusion analysis using a dynamic contrast-enhanced inversion-prepared dual-contrast gradient echo sequence. Invest Radiol 2008; 43: 481–487.
43 Franiel T, Lüdemann L, TaupitzMet al. Pharmacokinetic MRI of the Prostate: Parameters for Differentiating Low-Grade and High-Grade Prostate Cancer. Fortschr Röntgenstr 2009; 181: 536–542.
44 Shukla-Dave A, Hricak H, Ishill NM et al. Correlation of MR imaging and MR spectroscopic imaging findings with Ki-67, phospho-Akt, and androgen receptor expression in prostate cancer. Radiology 2009; 250:803–812.
45 Mueller-Lisse UG, Swanson MG, Vigneron DB et al. Magnetic resonance spectroscopy in patients with locally confined prostate cancer: association of prostatic citrate and metabolic atrophy with time on hormone deprivation therapy, PSA level, and biopsy Gleason score. Eur Radiol 2007; 17: 371–378.
46 Fradet V, Kurhanewicz J, Cowan JE et al. Prostate cancer managed with active surveillance: role of anatomic MR imaging and MR spectroscopic imaging. Radiology 2010; 256: 176–183. DOI: radiol.10091147.
47 Verma S, Rajesh A, Futterer JJ et al. Prostate MRI and 3D MR spectroscopy: how we do it. Am J Roentgenol 2010; 194: 1414–1426.
48 Hoeks CMA, Barentsz JO, Hambrock T et al. Prostate cancer: multiparametric MR imaging for detection, localization, and staging. Radiology 2011; 261: 46–66.
49 Scheenen TWJ, Futterer J, Weiland E et al. Discriminating cancer from noncancer tissue in the prostate by 3-dimensional proton magnetic resonance spectroscopic imaging: a prospective multicenter validation study. Invest Radiol 2011; 46: 25–33.
50 Weinreb JC, Blume JD, Coakley FV et al. Prostate cancer: sextant localization at MR imaging and MR spectroscopic imaging before prostatectomy – results of ACRIN prospective multi-institutional clinicopathologic study. Radiology 2009; 251: 122–133. DOI: 251/1/122.
51 Futterer JJ, Scheenen TWJ, Heijmink SWTPJ et al. Standardized threshold approach using three-dimensional proton magnetic resonance spectroscopic imaging in prostate cancer localization of the entire prostate. Invest Radiol 2007; 42: 116–122.
52 Jung JA, Coakley FV, Vigneron DB et al. Prostate depiction at endorectal MR spectroscopic imaging: investigation of a standardized evaluation system. Radiology 2004; 233: 701–708.

Contact

Matthias Röthke, M.D.
Department of Radiology
German Cancer Research Center (DKFZ)
Im Neuenheimer Feld 280
69120 Heidelberg
Germany
Phone: +49(0)6221-422520
m.roethke@dkfz.de